International Journal of Heat and Mass Transfer 112 (2017) 597–606

Contents lists available at ScienceDirect

International Journal of Heat and Mass Transfer

journal homepage: www.elsevier.com/locate/ijhmt

Heat transfer and flow of a dense suspension between two cylinders

Wei-Tao Wu [a], Zhi-Fu Zhou [b], Nadine Aubry [c], James F. Antaki [a], Mehrdad Massoudi [d,*]

[a] Department of Biomedical Engineering, Carnegie Mellon University, Pittsburgh, PA 15213, USA
[b] State Key Laboratory of Multiphase Flow in Power Engineering, Xi'an Jiaotong University, Xi'an 710049, China
[c] Department of Mechanical and Industrial Engineering, Northeastern University, Boston, MA 02115, USA
[d] U.S. Department of Energy, National Energy Technology Laboratory (NETL), Pittsburgh, PA 15236, USA

ARTICLE INFO

Article history:
Received 13 January 2017
Received in revised form 3 May 2017
Accepted 4 May 2017

Keywords:
Concentrated suspension
Heat transfer
Non-homogeneous fluids
Rheology
Conduction

ABSTRACT

Concentrated suspensions, composed of solid particles and fluids, are used in many industrial applications. In this paper, we study the effects of temperature on the flow of a concentrated (dense) suspension between two long rotating cylinders. The viscosity of the suspension is assumed to depend on temperature and volume fraction of the solid particles. Based on these concepts, a generalized viscosity model is proposed and the model parameters are fitted with experimental data. The numerical results show good agreement with the available experimental measurements.

Published by Elsevier Ltd.

1. Introduction

Concentrated suspensions are complex fluids composed of solid particles dispersed in a fluid, and are important in many industrial applications, such as drilling fluids [1,2], ceramics and reinforced polymer composites [3], coal slurries [4,5], and food engineering [6], etc. Successful operation of these suspensions requires a thorough understanding of the thermo-rheological properties of the suspension, such as its viscosity, the particle distribution, and the impact of the temperature field, etc. [7–10].

Suspensions composed of particles in a fluid can be considered as multiphase materials, and specifically two-phase flow approach can be used to study them. When the amount of the dispersed (particle) phase is very small, not impacting the motion of the continuous (fluid) phase, then a "dilute phase approach", sometimes referred to as the Lagrangian-Eulerian approach can be used. This is a one-way coupling. Alternatively, when the two phases are interacting with each other influencing the motion and the behavior of each other, a "dense phase approach", sometimes called the Eulerian-Eulerian (or the two-fluid) approach can be used. This is a two-way coupling. In either approach, governing equations are written for each component, and constitutive relations are needed before one can solve a system of coupled differential equations to obtain the velocity, temperature fields, etc. [see Soo [11] and Marcus et al. [12], Massoudi [13,14]]. In addition to these two approaches, a macroscopic (global) approach can be taken; here the suspension is considered as a complex fluid whose properties depend on the volume fraction of the particles, among other parameters. In this paper we take this approach.

There are many published studies involving flow and heat transfer in suspensions [7,8,15–18]. For example, Ahuja [19] studied heat transfer in suspensions of polystyrene spheres in aqueous sodium chloride or glycerine; it was found that the thermal conductivity of the suspensions can be three times as much as the thermal conductivity of stationary suspensions. Shin and Lee [16] experimentally investigated the rheological and thermal behavior of dense suspensions in a shear flow where the effects of particle size, particle concentration and shear rate were studied. In their paper, a shear-thinning viscosity was observed; the thermal conductivity was found to be strongly affected by particle concentration and particle size. Chen and Louge [17] theoretically explored heat transfer enhancement of dense suspensions in fluids; heat transfer enhancement is thought to be related to the agitation and movement of the solid particles. This was modeled by coupling the fluid and the solid phases through a particle concentration source term. It is worth mentioning that in recent years, nanofluids, which are suspensions composed of base fluids with different types of nanoparticles, have received much attention for their unusual performance on enhancing heat transfer efficiency [20–25]. In general nanofluids are usually considered to be dilute suspensions,

* Corresponding author at: U.S. Department of Energy, National Energy Technology Laboratory (NETL), 626 Cochrans Mill Road, P.O. Box 10940, Pittsburgh, PA 15236, USA.

E-mail address: Mehrdad.Massoudi@NETL.DOE.GOV (M. Massoudi).

http://dx.doi.org/10.1016/j.ijheatmasstransfer.2017.05.017
0017-9310/Published by Elsevier Ltd.

and will not be discussed in this paper; for more details we refer to the recent review articles [23,26–29] and several important pioneering works [30–32].

In most situations, the suspension is modeled as a Bingham or as a power-law fluid model [33,34]. It is known that the rheological behavior of suspensions can be very complex. For example, the shear viscosity of a concentrated suspension, in addition to being dependent on the shear rate, could also depend on the volume fraction of the particles, the temperature, the pressure, etc. Krieger et al. [35], based on their experimental and theoretical studies for concentrated suspensions, suggested that the viscosity can depend on the shear rate and the volume fraction of the particles (with various sizes). According to their study, the shear-thinning property is dominant when the size of the (solid) particles is in the micro scale range, but this effect diminishes as the particle size increases. According to Briscoe et al. [36], the rheological behavior of concentrated suspensions, such as drilling mud, can also depend on pressure and temperature in applications, such as deep ocean drilling operations [37].

In this paper, we model the suspension as a non-linear fluid model where the shear viscosity depends on temperature and particle concentration, and particles migration is modeled by the concentration flux transport model proposed by Phillips et al. [38]. In Sections 2 and 3, the governing equations of motion and the constitutive relations for the stress tensor, the diffusive particle flux vector and the heat flux vector are provided. In Section 4, the numerical results are presented and analyzed. We first study the isothermal flow of a suspension between two concentric cylinders; we then consider effects of temperature and eccentricity.

2. Governing equations

If the effects of electro-magnetism and chemical reactions are ignored, the governing equations, for a suspension, are the conservation equations for mass, linear and angular momentum, particle concentration, and energy [7]. For a complete thermo-mechanical study, the entropy law should also be considered [see [39]].

2.1. Conservation of mass

$$\frac{\partial \rho}{\partial t} + div(\rho \boldsymbol{v}) = 0 \tag{1}$$

where ρ is the density of the suspension, $\partial/\partial t$ is the partial derivative with respect to time, and $\boldsymbol{v}$ is the velocity vector. For an isochoric motion, $div\boldsymbol{v} = 0$.

2.2. Conservation of linear momentum

$$\rho \frac{d\boldsymbol{v}}{dt} = div\boldsymbol{T} + \rho \boldsymbol{b} \tag{2}$$

where d/dt is the total time derivative, given by $d(\cdot)/dt = \partial(\cdot)/\partial t + [grad(\cdot)]\boldsymbol{v}$, $\boldsymbol{b}$ is the body force vector, and $\boldsymbol{T}$ is the Cauchy stress tensor. The conservation of angular momentum indicates that in the absence of couple stresses the stress tensor is symmetric, that is, $\boldsymbol{T} = \boldsymbol{T}^{\mathrm{T}}$.

2.3. Conservation of solid particles (particles flux)

$$\frac{\partial \phi}{\partial t} + \boldsymbol{v}\frac{\partial \phi}{\partial \boldsymbol{x}} = -div\boldsymbol{N} \tag{3}$$

The function ϕ is an independent kinematical field called the volume distribution or the volume fraction (related to concentration) with the property $0 \leqslant \phi(\mathrm{x},t) \leqslant \phi_{max} < 1$. Here the first term on the left hand side denotes the rate of accumulation of particles, the second term denotes the convected particle flux, and the term on the right hand side denotes the diffusive particle flux. Following [38], the diffusive particle flux $\boldsymbol{N}$ is composed of fluxes related to the Brownian motion, the variation of interaction frequency and the viscosity. Such a transport equation for the concentration of particles (convection-diffusion) has been widely used to study flow and heat transfer in suspensions [8,40,41].

2.4. Conservation of energy

For an incompressible fluid, the energy equation is,

$$\frac{\partial e}{\partial t} + div(e\boldsymbol{v}) = \boldsymbol{T} : \boldsymbol{L} - div\boldsymbol{q} + \rho r \tag{4}$$

where e is the internal energy, $\boldsymbol{L}$ is the gradient of velocity, $\boldsymbol{q}$ is the heat flux vector, and r is the specific radiant energy (which is not considered in this paper). Thermodynamical considerations require the application of the second law of thermodynamics or the entropy inequality. The local form of the entropy inequality is given by (Liu, p. 130):

$$\rho\dot{\eta} + div\boldsymbol{\varphi} - \rho s \geqslant 0 \tag{5}$$

where $\eta(\boldsymbol{x},t)$ is the specific entropy density, $\boldsymbol{\varphi}(\boldsymbol{x},t)$ is the entropy flux, and s is the entropy supply density due to external sources, and the superposed dot denotes the material time derivative. If it is assumed that $\boldsymbol{\varphi} = \frac{1}{\theta}\boldsymbol{q}$, and $s = \frac{1}{\theta}r$, where θ is the absolute temperature, then Eq. (5) reduces to the familiar Clausius-Duhem inequality

$$\rho\dot{\eta} + div\frac{\boldsymbol{q}}{\theta} - \rho\frac{r}{\theta} \geqslant 0 \tag{6}$$

Even though we do not consider the effects of the Clausius-Duhem inequality in this paper, for a complete thermo-mechanical study of a problem, the second law of thermodynamics has to be considered [39,42–44]. From the above equations, we can see that constitutive relations are needed for $\boldsymbol{T}$, $\boldsymbol{q}$, $\boldsymbol{N}$, and e. We ignore the effects of radiation. We will discuss these modeling issues in the next section.

3. Constitutive equations

3.1. Stress tensor

In general, we think, the constitutive equation for the stress tensor of a concentrated suspension should be given by a non-Newtonian (non-linear) model [see [45]] and it may include a viscous stress and a yield stress [see [7]]:

$$\boldsymbol{T} = \boldsymbol{T}_y + \boldsymbol{T}_v \tag{7}$$

where $\boldsymbol{T}_y$ is the yield stress and $\boldsymbol{T}_v$ is the viscous stress tensor. In this paper, we will not consider the effect of the yield stress and we assume that, in general, the viscous stress can be represented by a generalized power-law fluid model, where

$$\boldsymbol{T}_{\boldsymbol{v}} = -p\mathbf{1} + \mu_r(p,\theta)\left(1 - \frac{\phi}{\phi_{max}}\right)^{-\beta}\Pi^{\frac{m}{2}}\boldsymbol{D} \tag{8}$$

$$\mu_r = \mu_{r0}e^{\frac{C_{10}p\theta E_u - C_{20}p}{k_B(\theta-\theta_C)}} \tag{9}$$

$$\Pi = 2tr\boldsymbol{D}^2,\ \boldsymbol{D} = \frac{1}{2}(\boldsymbol{L} + \boldsymbol{L}^T),\ \boldsymbol{L} = grad\boldsymbol{v} \tag{10}$$

Here, $\mathbf{1}$ is the identity tensor, p is the pressure, θ is temperature, ϕ is the volume fraction, tr is the trace operator, Π is an invariant of $\boldsymbol{D}$ where $\boldsymbol{D}$ is the symmetric part of the velocity gradient, E_u is related to an "activation energy", k_B is the Boltzmann constant,

C_{10}, C_{10} and θ_c are constants related to the effect of temperature, and m is the power-law exponent. Also, in the above equation, we have separated the dependency of the shear viscosity on the pressure, the concentration, the temperature, and the shear rate, where, $\mu_r(p,T)$, $(1-\phi/\phi_{max})^{-\beta}$, and $\Pi^{\frac{m}{2}}$ represent the effect of pressure and temperature, volume fraction and shear-thinning (or shear-thickening), respectively. Also, when $m<0$, the fluid is shear-thinning, and when $m>0$, the fluid is shear-thickening. This model, to a large extent, depends on Krieger's work which provided a correlation for the viscosity of suspensions as a function of particle concentration $\left(\mu=\mu_r(1-\phi/\phi_m)^{-1.82}\right)$ [35], where ϕ_m is the maximum packing value for volume fraction, where the suspension begins to exhibit solid-like behavior. In the remainder of this study, we ignore the shear rate dependency of the viscosity. Note that in certain applications, such as blood flow, the shear-rate dependency of the viscosity cannot be ignored [46,47]. Furthermore we also ignore the dependency of μ on the pressure. In many applications, such as deep ocean drilling operations, polymer melts, slag, etc., this effect should be included [36,48–50]. The form of the stress tensor studied in this paper is,

$$\boldsymbol{T_v}=-p\mathbf{1}+\mu_{r0}e^{\frac{C_{10}\theta E_u-C_{20}}{k_B(\theta-\theta_c)}}\left(1-\frac{\phi}{\phi_{max}}\right)^{-\beta}\boldsymbol{D} \tag{11}$$

As shown in Eq. (8), the viscosity is a function of the particle concentration and temperature, and if $\beta=2.5$, the model obeys the Einstein-Roscoe relation [51,52]. We should mention that there are alternative ways of modeling non-homogenous suspensions [see for instance Massoudi and Vaidya [53,54]]. In Section 3.2 we discuss the modeling of the particle flux $\boldsymbol{N}$.

3.2. Particle flux

As noted by [9], the particle transport flux, in the volume fraction equation, can be due to sedimentation, the Brownian motion, etc. In this study, due to the large size of the particles, we ignore the Brownian motion. Then the diffusive particle flux becomes:

$$\boldsymbol{N}=\boldsymbol{N}_c+\boldsymbol{N}_\mu \tag{12}$$

where $\boldsymbol{N}_c$ is the flux due to particle interactions and $\boldsymbol{N}_\mu$ is the flux associated with spatial variations in the viscosity. Based on [38], we assume:

$$\boldsymbol{N}_c=-a^2\phi K_c\nabla(\dot{\gamma}\phi) \tag{13}$$

$$\boldsymbol{N}_\mu=-a^2\phi^2\dot{\gamma}K_\mu\nabla(ln\mu) \tag{14}$$

$$\dot{\gamma}=(2D_{ij}D_{ij})^{1/2}=(\Pi)^2 \tag{15}$$

where a is the characteristic length associated with the particles (e.g. radius), ∇ is the gradient operator, $\dot{\gamma}$ is the local shear rate, μ is the effective viscosity, and K_c, K_μ are empirically-determined coefficients. According to Phillips et al. [38], $\boldsymbol{N}_c$ accounts for the effect of the spatially varying interaction frequency due to collisions between particles, while $\boldsymbol{N}_\mu$ accounts for the effect of the spatially varying viscosity. Mathematically $\boldsymbol{N}_c$ and $\boldsymbol{N}_\mu$ are responsible for the particles migration, causing non-homogenous distribution of the particles. Seifu et al. [55] noted that the particle flux could be expressed as,

$$\boldsymbol{N}=-a^2K_c\phi^2\dot{\gamma}\nabla\left(ln\left(\dot{\gamma}\phi\mu^{K_\mu/K_c}\right)\right) \tag{16}$$

We can see that $ln(\dot{\gamma}\phi\mu^{K_\mu/K_c})$ is a field potential incorporating mechanisms that can cause migration of particles. Phillips et al. and Subia et al. [9,38] assumed that K_c, K_μ, are constants. In this paper, we apply the empirical correlation proposed by Tetlow et al. [40],

$$\frac{K_c}{K_\mu}=1.25\phi+0.075 \tag{17}$$

where $K_\mu=0.62$, and the two constants in Eq. (17) were fitted with the experiments performed by Tetlow et al. [40]. Next we discuss the modeling of e, the specific internal energy.

3.3. Internal energy

In general, the internal energy density is related to the specific internal energy ε and is given by,

$$e=\rho\varepsilon \tag{18}$$

As shown by Dunn and Fosdick [56] for a second grade fluid, the specific internal energy ε is related to the specific Helmholtz free energy Ψ through:

$$\varepsilon=\Psi+\theta\eta=\varepsilon(\theta,\boldsymbol{A}_1,\boldsymbol{A}_2) \tag{19}$$

where $\boldsymbol{A}_1$ and $\boldsymbol{A}_2$ are the first and second Rivlin-Ericken tensors, where $\boldsymbol{A}_1=\boldsymbol{L}+\boldsymbol{L}^{\mathbf{T}}$, $\boldsymbol{A}_2=\frac{d\boldsymbol{A}_1}{dt}+\boldsymbol{A}_1\boldsymbol{L}+\boldsymbol{L}^T\boldsymbol{A}_1, \eta$ is the specific entropy and θ is the temperature [57]. In this paper, we simply assume that

$$\varepsilon=c_p\theta \tag{20}$$

where c_p is the specific heat capacity of the suspension. Substitute Eq. (20) into (18) and allowing for c_p to be weighted by ϕ, we have,

$$e=\left[(1-\phi)\rho_{f0}c_{pf0}+\phi\rho_{s0}c_{ps0}\right]\theta \tag{21}$$

where c_{pf0} and c_{ps0} are the specific heat capacity of the pure fluid (with no particles) and the solid particles, respectively. Next, we discuss the modeling of the heat flux vector.

3.4. Heat flux vector

The classical theory of heat conduction, first proposed by Fourier [58] (see also Winterton [59]) states that the heat flux vector is related to the temperature gradient, where

$$\boldsymbol{q}=-k\nabla\theta \tag{22}$$

where k is the thermal conductivity of the material. For complex materials, k can depend on concentration, temperature, etc., and in fact, k becomes a second order tensor for anisotropic materials. [For more information about the effective thermal conductivity concept in porous media and multiphase flows, see [60] (p.129) and [61–63]]. In this paper, we use Eq. (22) and assume that k can be replaced by an effective thermal conductivity. Jeffrey [64] derived an expression for the effective thermal conductivity which includes the second order effects in the volume fraction [65]:

$$k=\kappa_M\left[1+3\xi\phi+\hat{\xi}\phi^2\right]+O(\phi^3) \tag{23}$$

Table 1
Boundary conditions.

Boundary	Pressure	Velocity	Volume fraction	Temperature
Inner wall	Fixed flux (0)	Fixed value (ΩR_i)	Fixed flux (0)	Fixed value
Outer wall	Fixed flux (0)	Fixed value (0)	Fixed flux (0)	Fixed value

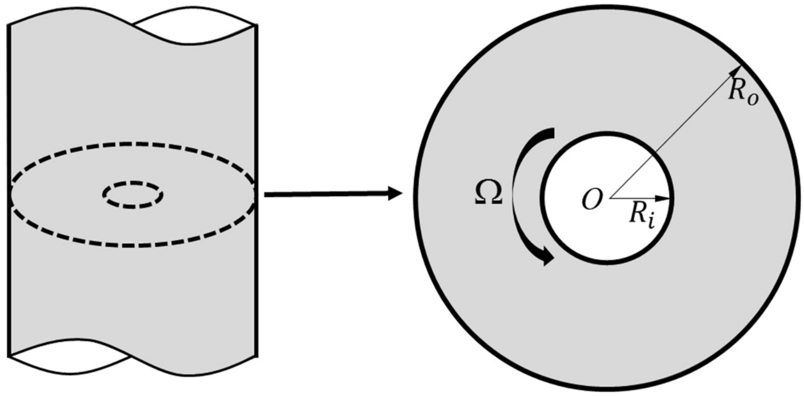

Fig. 1. Geometry of the two concentric cylinders. The radii of the inner and the outer cylinders are 0.64 cm and 2.38 cm, respectively. The rotational speed of the inner cylinder is 60 RPM [40].

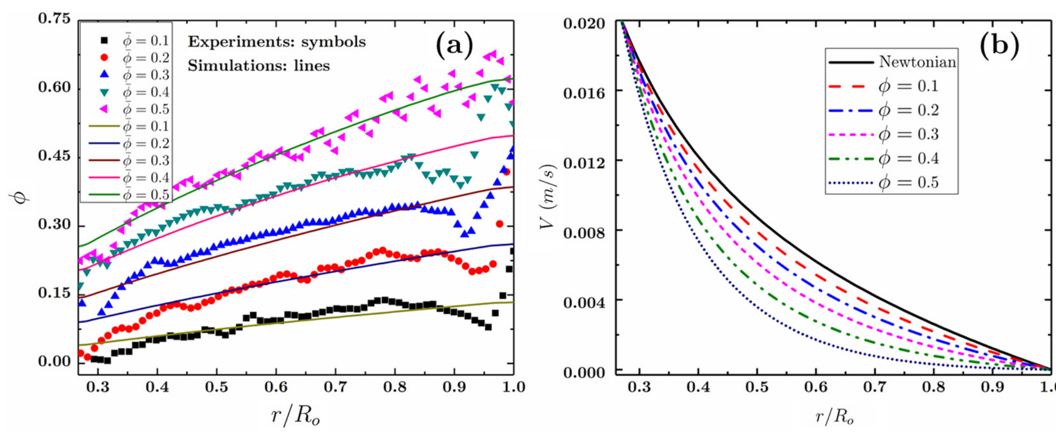

Fig. 2. (a) Steady-state volume fraction profiles obtained by simulations and compared with the experiment of [40] and (b) velocity profiles by simulations when the bulk volume fraction, $\bar{\phi}$, is 0.1, 0.2, 0.3, 0.4 and 0.5 and when the diameter of the suspened particles is 1.497 mm.

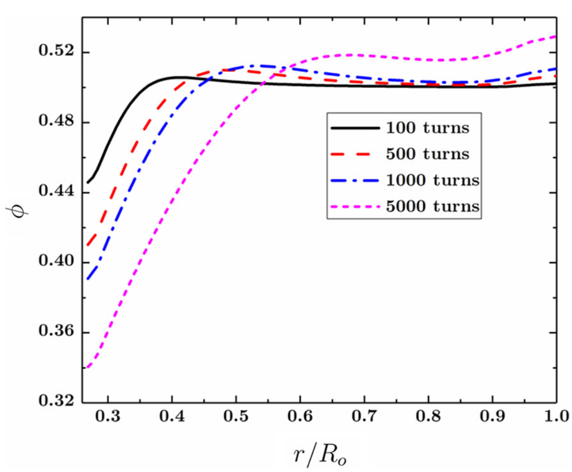

Fig. 3. Development of the volume fraction profiles in the region between the two concentric cylinders after the rotation of the inner cylinder has started, when the bulk volume fraction, $\bar{\phi}$, is 0.5 and the diameter of the suspened particles is 0.128 mm.

where

$$\hat{\xi} = 3\xi^2 + \frac{3\xi^3}{4} + \frac{9\xi^3}{16}\left(\frac{\omega+2}{2\omega+3}\right) + \frac{3\xi^4}{26} + \ldots \tag{24}$$

where

$$\xi = \frac{\omega - 1}{\omega + 2} \tag{25}$$

$$\omega = \frac{k_2}{k_1} \tag{26}$$

where ω is the ratio of conductivity of the particle to that of the matrix, k_M *is* the conductivity of the matrix (fluid). More recently, Pabst [66] has derived a relationship for the effective thermal conductivity of a suspension,

$$k = 1 - \frac{3}{2}\phi + \frac{1}{2}\phi^2 \tag{27}$$

In this paper we will use Eqs. (22)–(26).

4. Results and discussion

Using Eqs. (7)–(10), (12)–(17) and (21)–(26) in Eqs. (1)–(4), we obtain a set of partial differential equations which need to be solved numerically. To obtain numerical solutions to the governing equations, we build our PDEs solver using the libraries provided by OpenFOAM [67]. In the following sections, we first look at the isothermal flow of a suspension between two rotating cylinders; later in the paper, we consider the effect of temperature on the suspension flow. The PDEs are given below:

$$\frac{\partial \rho}{\partial t} + div(\rho \boldsymbol{v}) = 0 \tag{28}$$

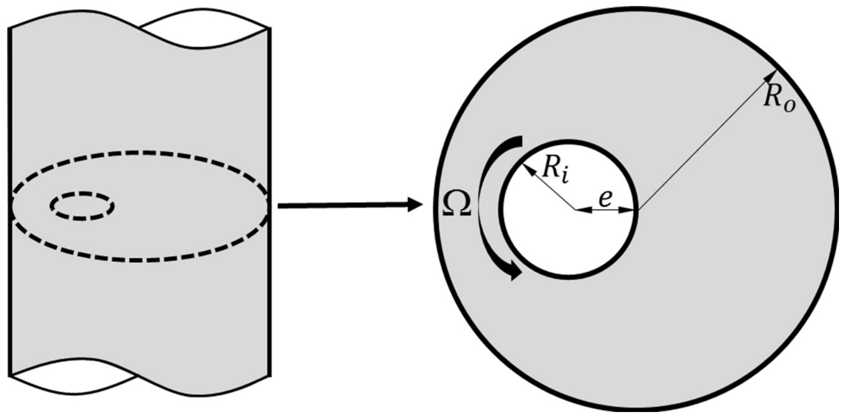

Fig. 4. Geometry of the two eccentric cylinders. The radii of the inner and the outer cylinders are 0.64 cm and 2.54 cm, respectively. The eccentricity ratio is $\epsilon = E/(R_o - R_i) = 0.5$. E is the distance between the center of two cylinders. The rotational speed of the inner cylinder is 90 RPM.

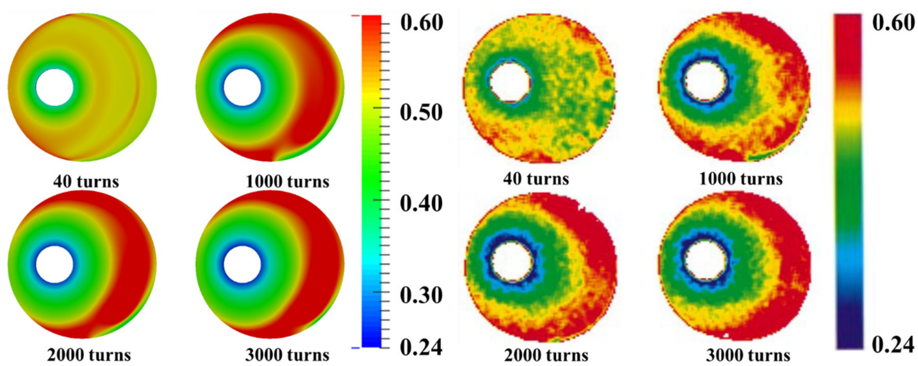

Fig. 5. The evolution of the volume fraction field as the inner cylinder rotates using our simulation (left) and experiment (right) [9]. The experimental results are reused by permission.

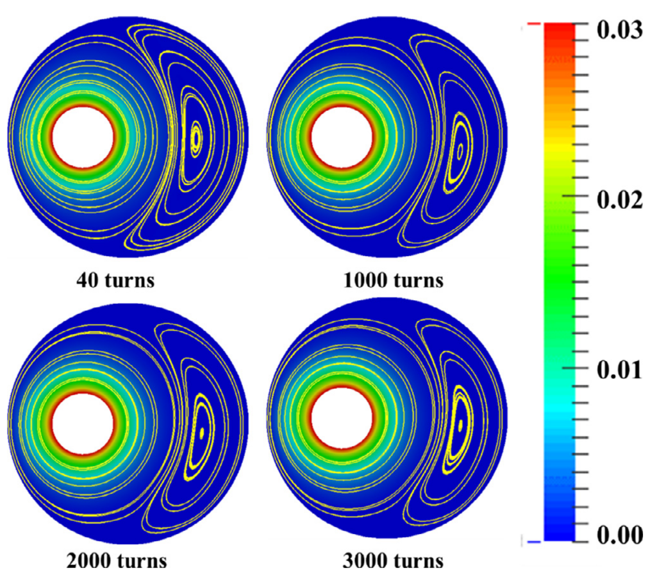

Fig. 6. Streamlines and velocity fields at different RPMs.

$$\rho\left(\frac{\partial \boldsymbol{v}}{\partial t} + (grad\,\boldsymbol{v})\boldsymbol{v}\right) = -grad p + div(\mu_{r0} e^{\frac{C_{10}\theta E_u - C_{20}}{k_B(\theta - \theta_c)}}\left(1 - \frac{\phi}{\phi_{max}}\right)^{-\beta}\boldsymbol{D}) \tag{29}$$

$$\frac{\partial \phi}{\partial t} + \boldsymbol{v}\frac{\partial \phi}{\partial \boldsymbol{x}} = div(a^2\phi K_c \dot{\gamma}\nabla(\phi)) + div(a^2\phi K_c \nabla(\dot{\gamma})\phi + a^2\dot{\gamma}K_\mu \nabla(ln\mu)\phi^2) \tag{30}$$

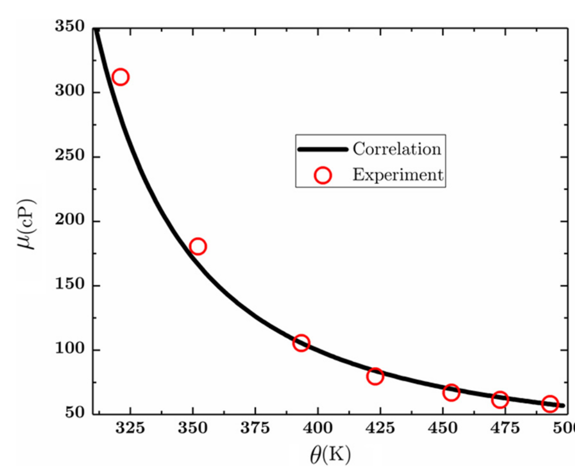

Fig. 7. Viscosity as a function of temperature. The average volume fraction of the solid particles is 0.345. The suspension is made of water, various additives and solid particles, and its density is 2.2 g/cm^3.

$$\left((1-\phi)\rho_{f0}C_{pf0} + \phi\rho_{s0}C_{ps0}\right)\left(\frac{\partial \theta}{\partial t} + (grad\theta)\boldsymbol{v}\right) = \left(\mu_r(p,T)\left(1 - \frac{\phi}{\phi_{max}}\right)^{-\beta}\boldsymbol{D}\right) : \boldsymbol{L} + div\left(\kappa_M(1 + 3\xi\phi + \hat{\xi}\phi^2)\nabla\theta\right) \tag{31}$$

Subject to the boundary conditions shown in Table 1:

For each geometry, a mesh (in)dependency study is performed. We consider two-dimensional flows, where the velocity, the volume fraction and the temperature fields, using the Cartesian coordinate system (x, y, z), are assumed to be given by:

$$\begin{cases} v = v_x(x, y; t)\boldsymbol{e_x} + v_y(x, y; t)\boldsymbol{e_y} \\ \phi = \phi(x, y; t) \\ \theta = \theta(x, y; t) \end{cases} \quad (32)$$

4.1. Isothermal flow between two rotating cylinders

4.1.1. Concentric cylinders

Flow of a suspension between two rotating cylinders occurs in many industrial application such as journal bearing [68,69] and drilling fluid between the drill pipe and the casing [2,70]. The geometry can be idealized as shown in Fig. 1. We assume that the radii of the two cylinders are 0.64 cm and 2.38 cm, the viscosity of the suspending fluid (μ_r) is 2.1 Pa s at 28 °C, the diameter of the suspened particles is 1.497 mm and the inner cylinder rotates at 60 RPM (These values are based on the experiments of [40]). Tetlow et al. looked at this problem by assuming a fully developed Couette flow; they obtained a good agreement between their numerical predictions and their experimental measurements [40]. Fig. 2 shows the results for steady-state flow by comparing the numerically obtained volume fraction and velocity profiles and experimental observations when the bulk volume fraction, $\bar{\phi}$, is 0.1, 0.2, 0.3, 0.4 and 0.5 [40]. For the details of the experimental techniques, see [40]. It can be seen that the results of our simulation match reasonably well with the experimental observations. We also notice a non-linear velocity profile when $\bar{\phi} = 0.5$. Furthermore as $\bar{\phi}$ decreases the particle volume fraction profiles gradually lose their non-linearity and the velocity profiles become similar to the case of the Newtonian fluid implying the fluid behaves more like a linear fluid as the particle volume fraction decreases.

Fig. 3 shows the development of the volume fraction profiles after the rotation of the inner cylinder has started, with bulk volume fraction, $\bar{\phi} = 0.5$. To show the particle migration more clearly, we consider smaller sized particles, for example, a 0.128 mm diameter. As the inner cylinder begins to rotate the particles gradually move toward the outer cylinder; this is more obvious near the cylinder walls. That is, particles migration is more intense at the start of the motion.

4.1.2. Eccentric cylinders

It is well known that the effect of the eccentricity on the flow between two rotating cylinders can be significant [2]. Fig. 4 shows the geometry where the inner and the outer cylinder radii are 0.64 cm and 2.54 cm, respectively, and the eccentricity ratio is $\epsilon = E/(R_o - R_i) = 0.5$, where E is the distance between the centers of the two cylinders. Here we assume that the inner cylinder rotates at 90 RPM, and the bulk volume fraction, $\bar{\phi}$, is 0.5 [9].

Fig. 5 shows the variation of the particle volume fraction field, using simulations, for different numbers of revolutions of the inner cylinder. The experimental data can be found in [9]. A good agreement has been achieved between simulations and experiments. Both results show that after the inner cylinder has started rotating, the particles gradually begin to move to the outer (stationary) cylinder. After a large number of revolutions of the inner cylinder, such as 3000, it is observed [see Fig. 5] that a particle depletion zone near the rotating cylinder and a zone with a high particle

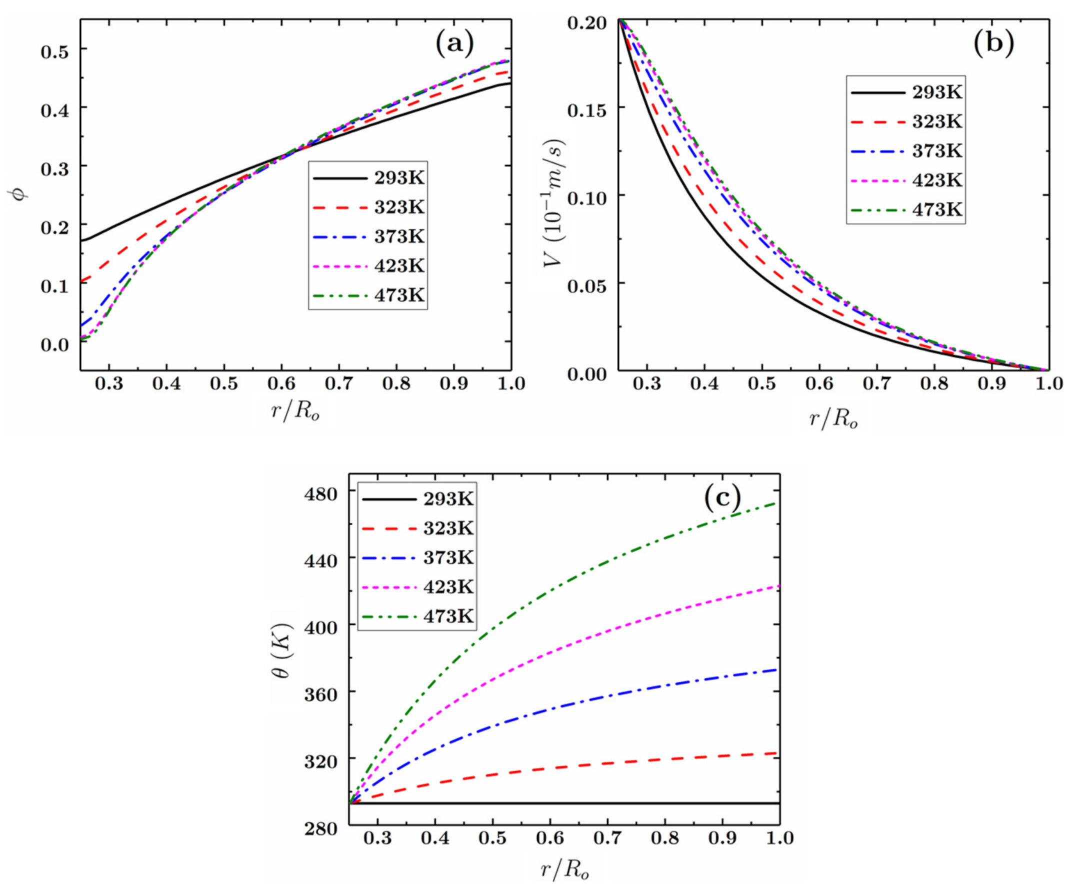

Fig. 8. (a) The particle concentration, (b) the velocity and (c) the temperature profiles for different values of the outer wall temperature. The temperature of the inner wall is 293 K.

concentration in the wide-gap region between the two cylinders appear.

Fig. 6 shows the streamlines and the velocity fields. We can see the emergence of two different flow patterns: one is the (main) flow region around the inner cylinder and the other is the recirculation/secondary flow region in the wide gap. A similar pattern is also observed for the volume fraction field as shown in Fig. 5. The streamlines for the main flow region are similar to the flow pattern between the two concentric cylinders. The velocity in the recirculation zone is very small, which leads to a low local shear rate distribution. According to Eq. (16), due to the low shear rate, the field potential in the circulation zone is small and this causes a particle flux variation from the main stream to the circulation region where we notice a high particle concentration.

4.2. Flow and heat transfer between two rotating cylinders

In many engineering problems, the effects of temperature on the flow field needs to be considered, for example the flow of nanofluids [71], the bearing load [68], and the flow of drilling fluids [36]. In this part of the paper we consider the flow of a suspension under non-isothermal conditions. The values of the material parameters in Eq. (8) are fitted using the experimental measurements of Wang et al. [72]: $\mu_{r0} = 0.4153$ cP, $C_1 = \frac{C_{10}E_u}{k_B} = 2.3981$, $C_2 = \frac{C_{20}}{k_B} = 46.3226$ K and $\theta_c = 182.3742$ K. In their measurements, the shear rate varied from 0 to 1020 s^{-1}; the shear viscosity was found to be independent of the shear rate, see Wang et al. [72]. Comparison between the fitted expression and the experimental data are shown in Fig. 7. The bulk volume fraction is 0.345. The density of the (drilling) suspension is 2.2 g/cm^3 and it is composed of water, various additives and solid particles. The particle density is 4.48 g/cm^3. κ_M and ω are chosen as 0.6485 W/(m^{-1} K^{-1}) and 2.0, respectively [73]. The diameter of the solid particles is kept the same, i.e., 1.497 mm. We assume that the wall temperatures of the inner (θ_i) and the outer cylinders (θ_o) are given. That is, we assume constant temperature boundary conditions at both the

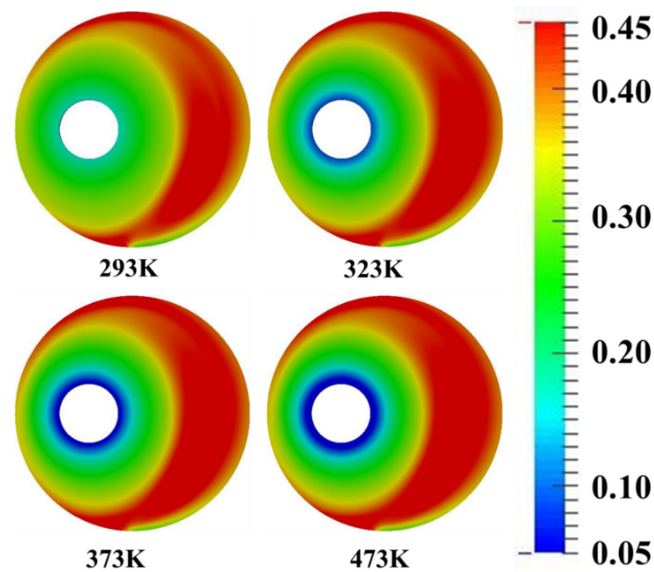

Fig. 10. Volume fraction fields for different values of the wall temperature of the outer cylinder. The inner wall temperature is 293 K.

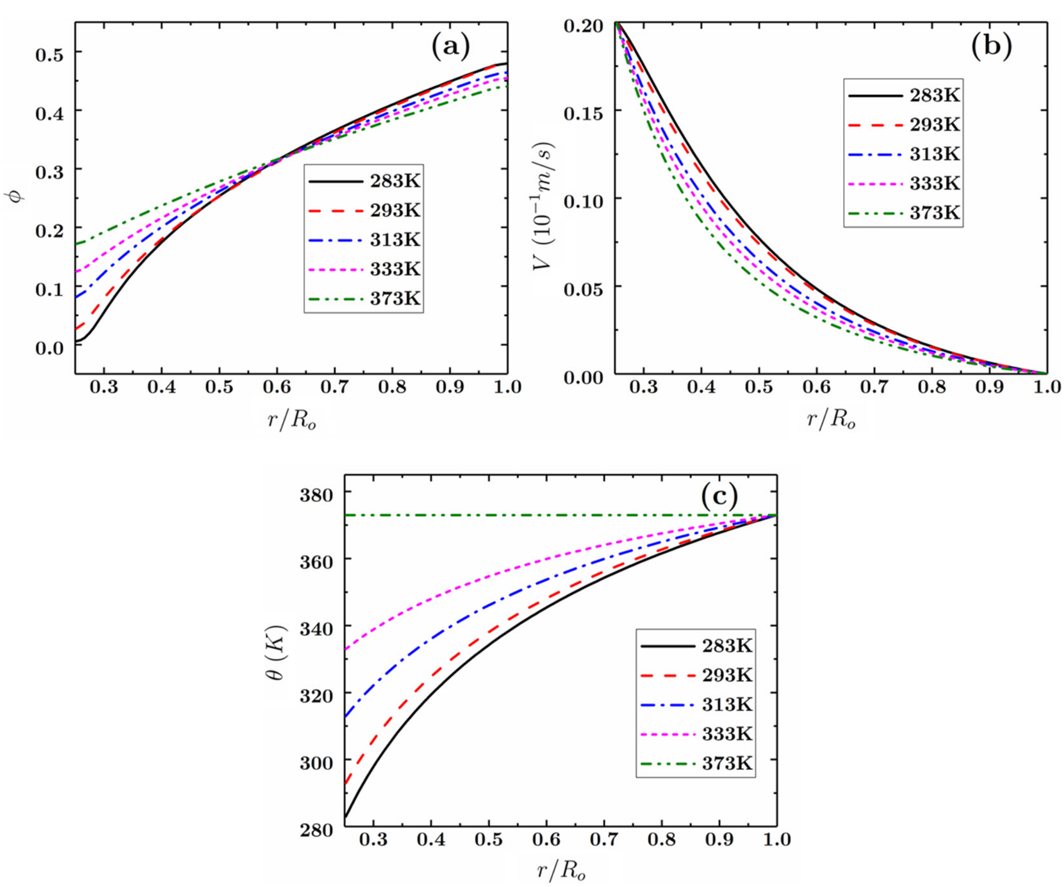

Fig. 9. (a) Particle concentration, (b) velocity and (c) temperature profiles for different values of the inner wall temperature. The temperature of the outer wall is 373 K.

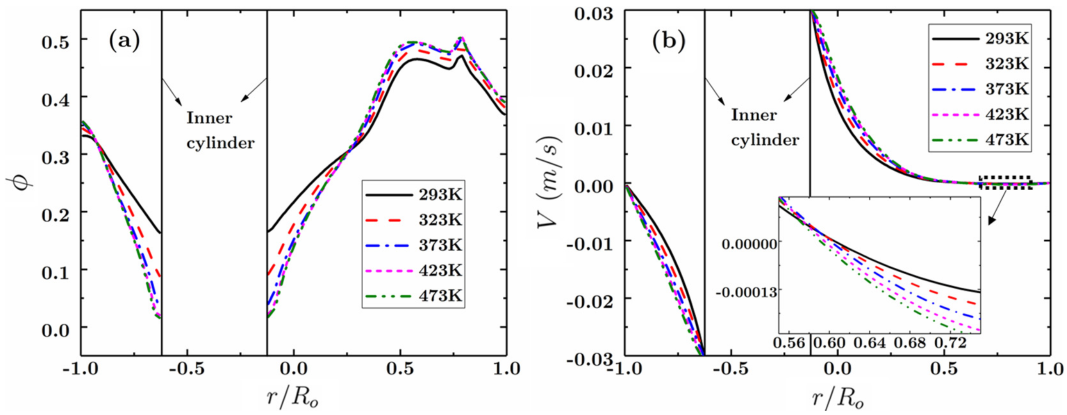

Fig. 11. (a) Volume fraction profiles for different values of the wall temperature of the outer cylinder; (b) Velocity profiles for different values of the wall temperature of the outer cylinder. The inner wall temperature is 293 K.

cylinder walls. In addition, all other flow conditions, such the rotating speed of the inner wall, etc., are the same as the previous cases.

4.2.1. Concentric cylinders

Fig. 8 shows the profiles for the particle volume fraction, velocity and temperature for different values of the wall temperature of the outer cylinder. From Fig. 8(a), we can see that as the wall temperature of the outer cylinder increases, the volume fraction distribution becomes more non-uniform, where the particle concentration near the inner wall drops dramatically. From Fig. 8 (b) we also observe that a lower temperature for the outer cylinder produces some nonlinearity in the velocity profiles. This may be attributed to the competing effects between the volume fraction and the temperature on the suspension viscosity: the value of the volume fraction and temperature increase along the radial direction, while according to Eqs. (8) and (9) they have the opposite effect on the suspension viscosity. This may cause a more uniform viscosity distribution as the temperature difference between the inner and the outer walls increases. Fig. 8(c) shows the profiles for the temperature distribution. As the temperature for the outer wall changes we observe that the temperature distribution becomes a bit more nonlinear.

Fig. 9 shows the effect of changing the inner wall temperature. Comparing Figs. 8 and 9, we can see that the effect of the inner and the outer wall temperatures on the flow pattern are similar. That is, when the temperature of the inner and the outer walls are identical, the profiles for the volume fraction and the velocity distribution are similar. From the results of our previous parametric studies [8], we know that for the case of steady-state Couette flow, the temperature gradient has an effect on the flow field. Therefore, we may conclude here that the temperature difference between the inner and the outer cylinders influences the flow pattern.

4.2.2. Eccentric cylinders

The geometry is shown in Fig. 4. Fig. 10 shows the particle concentration field for different values of the outer wall temperature. As the outer wall temperature changes, the pattern for the volume fraction field does not change much. Near the inner cylinder, the volume fraction is the smallest, and there exists a region in the wide gap with high particle concentration. We also notice that the volume fraction field changes more dramatically near the inner cylinder.

Fig. 11 shows the concentration and the velocity profiles for different values of the outer wall temperature. In general, along the radial direction for the narrow-gap and for a large portion of the wide-gap between the two cylinders, there is a gradual increase in the values of the particle volume fraction; this is similar to the case of the two concentric cylinders. Interestingly, for the cases presented here, near the outer wall, there are two peaks for the concentration, see Figs. 5 and 6. These two peaks may be attributed to: (1) Secondary flow and flow circulation which contribute to particle sedimentation; (2) The high particle concentration in the narrow gap is convected to the middle of the wide gap and forms a thin layer of high particle concentration. For the velocity profiles shown in Fig. 11(b), a flow separation is observed in the wide-gap region.

5. Conclusions

The results of our simulations are compared with the available experiments for the isothermal condition. For cases with non-uniform temperature field, the viscosity term is fitted with the experimental data. We have looked at a two–dimensional flow between two long vertical pipes, and therefore the effect of gravity is ignored. For inclined or horizontal flows, solid particles may settle (due to gravity). For these types of processes, transport flux of solid particles caused by gravity should also be included in the flux equation (for more information see [74–76]). We have studied the flow and heat transfer in dense suspensions between two rotating concentric and eccentric cylinders. Based on the work of Briscoe et al. [36], Krieger [35], a generalized viscosity model which depends on the volume fraction, temperature and the shear rate is proposed; the parameters are fitted with the available experimental data. The volume fraction distribution is obtained by using a concentration flux transport model. The results indicate a good agreement between the experiments and the numerical simulations. Through these numerical simulations, we find that the temperature field has an obvious effect on the flow. For the flow between two eccentric cylinders, the temperature difference between the inner and the outer cylinders creates a layer of low particle concentration near the inner cylinder.

References

[1] H. Rabia, Oilwell Drilling Engineering: Principles and Practice, Graham and Trotman Ltd, London, 1985.
[2] D.A. Siginer, S.I. Bakhtiyarov, Flow of drilling fluids in eccentric annuli, J. Nonnewton. Fluid Mech. 78 (1998) 119–132.
[3] R.C. Givler, M.J. Crochet, R.B. Pipes, Numerical prediction of fiber orientation in dilute suspensions, J. Compos. Mater. 17 (1983) 330–343.
[4] W.-T. Wu, N. Aubry, M. Massoudi, On the coefficients of the interaction forces in a two-phase flow of a fluid infused with particles, Int. J. Non. Linear. Mech. 59 (2014) 76–82.
[5] T.A. Özbelge, Heat transfer enhancement in turbulent upward flows of liquid–solid suspensions through vertical annuli, Int. J. Heat Mass Transf. 44 (2001) 3373–3379.

[6] M. Gradeck, B.F.Z. Fagla, C. Baravian, M. Lebouché, Experimental thermomechanic study of Newtonian and non-Newtonian suspension flows, Int. J. Heat Mass Transf. 48 (2005) 3469–3477.
[7] Z. Zhou, W.-T. Wu, M. Massoudi, Fully developed flow of a drilling fluid between two rotating cylinders, Appl. Math. Comput. 281 (2016) 266–277. <http://www.sciencedirect.com/science/article/pii/S0096300316300686> (accessed February 22, 2016).
[8] W.-T. Wu, M. Massoudi, Heat transfer and dissipation effects in the flow of a drilling fluid, Fluids 1 (2016) 4. <http://www.mdpi.com/2311-5521/1/1/4/htm> (accessed April 4, 2016).
[9] S.R. Subia, M.S. Ingber, L.A. Mondy, S.A. Altobelli, A.L. Graham, Modelling of concentrated suspensions using a continuum constitutive equation, J. Fluid Mech. 373 (1998) 193–219.
[10] M. Massoudi, A.K. Uguz, Chemically-reacting fluids with variable transport properties, Appl. Math. Comput. 219 (2012) 1761–1775.
[11] S. Soo, Fluid dynamics of multiphase systems, 1967.
[12] R.D. Marcus, L.S. Leung, G.E. Klinzing, F. Rizk, Pneumatic Conveying of Solids, Chapman and Hall, London, 1990.
[13] M. Massoudi, A note on the meaning of mixture viscosity using the classical continuum theories of mixtures, Int. J. Eng. Sci. 46 (2008) 677–689.
[14] M. Massoudi, A Mixture Theory formulation for hydraulic or pneumatic transport of solid particles, Int. J. Eng. Sci. 48 (2010) 1440–1461.
[15] S.N. Kazi, G.G. Duffy, X.D. Chen, Study of the effect of entrance length on heat transfer to fibre suspensions in annular flow heat exchangers, Int. J. Heat Mass Transf. 78 (2014) 548–556.
[16] S. Shin, S.-H. Lee, Thermal conductivity of suspensions in shear flow fields, Int. J. Heat Mass Transf. 43 (2000) 4275–4284.
[17] X. Chen, M. Louge, Heat transfer enhancement in dense suspensions of agitated solids. Part I: Theory, Int. J. Heat Mass Transf. 51 (2008) 5108–5118.
[18] G. Flamant, D. Gauthier, H. Benoit, J.-L. Sans, R. Garcia, B. Boissière, R. Ansart, M. Hemati, Dense suspension of solid particles as a new heat transfer fluid for concentrated solar thermal plants: on-sun proof of concept, Chem. Eng. Sci. 102 (2013) 567–576.
[19] A.S. Ahuja, Augmentation of heat transport in laminar flow of polystyrene suspensions. I. Experiments and results, J. Appl. Phys. 46 (1975) 3408–3416.
[20] M.R. Safaei, G. Ahmadi, M.S. Goodarzi, M. Safdari Shadloo, H.R. Goshayeshi, M. Dahari, Heat transfer and pressure drop in fully developed turbulent flows of graphene nanoplatelets–silver/water nanofluids, Fluids 1 (2016) 20.
[21] M.R. Safaei, G. Ahmadi, M.S. Goodarzi, A. Kamyar, S.N. Kazi, Boundary layer flow and heat transfer of FMWCNT/water nanofluids over a flat plate, Fluids 1 (2016) 31.
[22] B. Gu, B. Hou, Z. Lu, Z. Wang, S. Chen, Thermal conductivity of nanofluids containing high aspect ratio fillers, Int. J. Heat Mass Transf. 64 (2013) 108–114.
[23] A. Kasaeian, R.D. Azarian, O. Mahian, L. Kolsi, A.J. Chamkha, S. Wongwises, I. Pop, Nanofluid flow and heat transfer in porous media: a review of the latest developments, Int. J. Heat Mass Transf. 107 (2017) 778–791.
[24] W.-T. Wu, M. Massoudi, H. Yan, Heat transfer and flow of nanofluids in a Y-type intersection channel with multiple pulsations: a numerical study, Energies 10 (2017) 492.
[25] D. Wen, Y. Ding, Experimental investigation into convective heat transfer of nanofluids at the entrance region under laminar flow conditions, Int. J. Heat Mass Transf. 47 (2004) 5181–5188.
[26] X.-Q. Wang, A.S. Mujumdar, Heat transfer characteristics of nanofluids: a review, Int. J. Therm. Sci. 46 (2007) 1–19.
[27] S.U.S. Choi, Z.G. Zhang, W. Yu, F.E. Lockwood, E.A. Grulke, Anomalous thermal conductivity enhancement in nanotube suspensions, Appl. Phys. Lett. 79 (2001) 2252–2254.
[28] X. Fang, Y. Chen, H. Zhang, W. Chen, A. Dong, R. Wang, Heat transfer and critical heat flux of nanofluid boiling: a comprehensive review, Renew. Sustain. Energy Rev. 62 (2016) 924–940.
[29] M.B. Bigdeli, M. Fasano, A. Cardellini, E. Chiavazzo, P. Asinari, A review on the heat and mass transfer phenomena in nanofluid coolants with special focus on automotive applications, Renew. Sustain. Energy Rev. 60 (2016) 1615–1633.
[30] S.U.S. Chol, Enhancing thermal conductivity of fluids with nanoparticles, ASME-Publications-Fed 231 (1995) 99–106.
[31] J.A. Eastman, U.S. Choi, S. Li, L.J. Thompson, S. Lee, Enhanced thermal conductivity through the development of nanofluids, in: MRS Proc., Cambridge University Press, Cambridge, UK, 1996, p. 3.
[32] Y. Xuan, Q. Li, Heat transfer enhancement of nanofluids, Int. J. Heat Fluid Flow 21 (2000) 58–64.
[33] C. Macosko, Rheology: Principles, Measurements and Applications, Wiley, New York, 1996.
[34] J. Málek, K.R. Rajagopal, M. Růžička, Existence and regularity of solutions and the stability of the rest state for fluids with shear dependent viscosity, Math. Model. Methods Appl. Sci. 5 (1995) 789–812.
[35] I.M. Krieger, Rheology of monodisperse latices, Adv. Coll. Interf. Sci. 3 (1972) 111–136.
[36] B.J. Briscoe, P.F. Luckham, S.R. Ren, The properties of drilling muds at high pressures and high temperatures, Philos. Trans. R. Soc. London A Math. Phys. Eng. Sci. 348 (1994) 179–207.
[37] L. Richardson, B. Straughan, Convection with temperature dependent viscosity in a porous medium: nonlinear stability and the Brinkman effect, Atti Della Accad. Naz. Dei Lincei. Cl. Di Sci. Fis. Mat. E Nat. Rend. Lincei. Mat. E Appl. 4 (1993) 223–230.
[38] R.J. Phillips, R.C. Armstrong, R.A. Brown, A.L. Graham, J.R. Abbott, A constitutive equation for concentrated suspensions that accounts for shear-induced particle migration, Phys. Fluids A Fluid Dyn. 4 (1992) 30–40.
[39] I.-S. Liu, Continuum Mechanics, Springer Science & Business Media, Berlin, Germany, 2002.
[40] N. Tetlow, A.L. Graham, M.S. Ingber, S.R. Subia, L.A. Mondy, S.A. Altobelli, Particle migration in a Couette apparatus: experiment and modeling, J. Rheol. 42 (1998) 307–327.
[41] M. Khan, A revised model to analyze the heat and mass transfer mechanisms in the flow of Carreau nanofluids, Int. J. Heat Mass Transf. 103 (2016) 291–297.
[42] I. Müller, On the entropy inequality, Arch. Ration. Mech. Anal. 26 (1967) 118–141.
[43] H. Ziegler, An Introduction to Thermomechanics, North-Holland Publishing Company, Amsterdam, The Netherlands, 1983.
[44] C. Truesdell, W. Noll, The Nonlinear Field Theories of Mechanics, Springer-Verlag, Berlin, 1992 (1965 & 1992).
[45] P.J. Carreau, D. De Kee, R.J. Chhabra, Rheology of Polymeric Systems, Hanser/Gardner Publications, Cincinnati, OH, 1997.
[46] W.-T. Wu, N. Aubry, M. Massoudi, J. Kim, J.F. Antaki, A numerical study of blood flow using mixture theory, Int. J. Eng. Sci. 76 (2014) 56–72.
[47] W.-T. Wu, F. Yang, J.F. Antaki, N. Aubry, M. Massoudi, Study of blood flow in several benchmark micro-channels using a two-fluid approach, Int. J. Eng. Sci. 95 (2015) 49–59. <http://www.sciencedirect.com/science/article/pii/S0020722515000890> (accessed February 29, 2016).
[48] G. Gupta, M. Massoudi, Flow of a generalized second grade fluid between heated plates, Acta Mech. 99 (1993) 21–33.
[49] L. Miao, M. Massoudi, Heat transfer analysis and flow of a slag-type fluid: effects of variable thermal conductivity and viscosity, Int. J. Non. Linear. Mech. 76 (2015) 8–19.
[50] L. Miao, W. Wu, N. Aubry, M. Massoudi, Falling film flow of a viscoelastic fluid along a wall, Math. Methods Appl. Sci. 37 (2013) 2840–2853.
[51] R. Roscoe, The viscosity of suspensions of rigid spheres, Br. J. Appl. Phys. 3 (1952) 267–269.
[52] R. Roscoe, in: J.J. Hermans (Ed.), Flow Prop. Disperse Syst., New York, NY, USA, 1953, pp. 1–38.
[53] M. Massoudi, A. Vaidya, Unsteady flows of inhomogeneous incompressible fluids, Int. J. Non. Linear. Mech. 46 (2011) 738–741.
[54] M. Massoudi, A. Vaidya, Analytical solutions to Stokes-type flows of inhomogeneous fluids, Appl. Math. Comput. 218 (2012) 6314–6329.
[55] B. Seifu, A. Nir, R. Semiat, Viscous dissipation rate in concentrated suspensions, Phys. Fluids 6 (1994) 3189–3191. <http://scitation.aip.org/content/aip/journal/pof2/6/9/10.1063/1.868098> (accessed April 6, 2016).
[56] J.E. Dunn, R.L. Fosdick, Thermodynamics, stability, and boundedness of fluids of complexity 2 and fluids of second grade, Arch. Ration. Mech. Anal. 56 (1974) 191–252.
[57] R.S. Rivlin, J.L. Ericksen, Stress-deformation relations for isotropic materials, J. Ration. Mech. Anal. 4 (1955) 323–425.
[58] J. Fourier, The Analytical Theory of Heat, Dover Publications, New York, 1955.
[59] R.H.S. Winterton, Early study of heat transfer: Newton and Fourier, Heat Transf. Eng. 22 (2001) 3–11.
[60] M. Kaviany, Principles of Heat Transfer in Porous Media, Springer, 1995.
[61] Y.M. Bashir, J.D. Goddard, Experiments on the conductivity of suspensions of ionically-conductive spheres, AIChE J. 36 (1990) 387–396.
[62] R.S. Prasher, P. Koning, J. Shipley, A. Devpura, Dependence of thermal conductivity and mechanical rigidity of particle-laden polymeric thermal interface material on particle volume fraction, J. Electron. Packag. 125 (2003) 386–391.
[63] D.-L. Lee, T.F. Irvine Jr., Shear rate dependent thermal conductivity measurements of non-Newtonian fluids, Exp. Therm. Fluid Sci. 15 (1997) 16–24.
[64] D.J. Jeffrey, Conduction through a random suspension of spheres, Proc. R. Soc. London. A. Math. Phys. Sci. 335 (1973) 355–367.
[65] G.K. Batchelor, R.W. O'Brien, Thermal or electrical conduction through a granular material, Proc. R. Soc. London. A. Math. Phys. Sci. 355 (1977) 313–333.
[66] W. Pabst, Simple second-order expression: for the porosity dependence of thermal conductivity, J. Mater. Sci. 40 (2005) 2667–2669.
[67] OpenCFD, OpenFOAM Programmer's Guide Version 2.1.0, CFD online Web Site, 2011.
[68] J.-S. Chen, K.-W. Chen, Bearing load analysis and control of a motorized high speed spindle, Int. J. Mach. Tools Manuf 45 (2005) 1487–1493.
[69] C.C. Shir, D.D. Joseph, Lubrication of a porous bearing—Reynolds' solution, J. Appl. Mech. 33 (1966) 761–767.
[70] R. Caenn, G.V. Chillingar, Drilling fluids: state of the art, J. Pet. Sci. Eng. 14 (1996) 221–230.
[71] C.T. Nguyen, F. Desgranges, G. Roy, N. Galanis, T. Maré, S. Boucher, H.A. Mintsa, Temperature and particle-size dependent viscosity data for water-based nanofluids–hysteresis phenomenon, Int. J. Heat Fluid Flow 28 (2007) 1492–1506.
[72] F. Wang, X. Tan, R. Wang, M. Sun, L. Wang, J. Liu, High temperature and high pressure rheological properties of high-density water-based drilling fluids for

deep wells, Pet. Sci. 9 (2012) 354–362. <http://link.springer.com/10.1007/s12182-012-0219-4> (accessed June 14, 2016).
[73] B. Yilmazer, Investigation of some physical and mechanical properties of concrete produced with barite aggregate, Sci. Res. Essays 5 (2010) 3826–3833.
[74] T. Hsu, P.A. Traykovski, G.C. Kineke, On modeling boundary layer and gravity-driven fluid mud transport, J. Geophys. Res. Ocean. 112 (2007).
[75] A. Acrivos, R. Mauri, X. Fan, Shear-induced resuspension in a Couette device, Int. J. Multiph. Flow 19 (1993) 797–802.
[76] A. Mavromoustaki, A.L. Bertozzi, Hyperbolic systems of conservation laws in gravity-driven, particle-laden thin-film flows, J. Eng. Math. 88 (2014) 29–48.